Hybrid Dyadic-Mixed-Potential and Combined Spectral-Space Domain Integral-Equation Analysis of Quasi-3-D Structures in Stratified Media

Mark Vrancken, *Member, IEEE,* and Guy A. E. Vandenbosch, *Member, IEEE*

***Abstract*—Planar circuits and antennas in stratified media are efficiently analyzed using an integral-equation formulation with a spectral-domain approach to construct the required Green's functions. This efficiency is largely lost when arbitrary three-dimensional (3-D) structures have to be analyzed. We, therefore, focus attention to "quasi 3-D" structures, which, although not fully 3-D, are still seen to cover most practical problems. The formulation of the electric field is adapted to the geometry as a hybrid dyadic-mixed-potential form. Evaluation of all z, z'-dependent parts of the reaction integrals is done analytically in the spectral domain. The remaining evaluation is done in the space domain with a mixed-potential formalism. We obtain a combined spectral-space domain approach to solve the integral equation. Numerical results demonstrate the applicability of the method to (most) 3-D problems that occur in planar stratified media.**

***Index Terms*—Dyadic, integral equation (IE), mixed potential, stratified medium, three-dimensional (3-D) planar.**

I. Introduction

In THE full-wave analysis of planar circuits, antennas, and interconnections in planar multilayered media, integral-equation (IE) formulations have shown higher efficiency than differential equation based methods like the finite-difference time-domain (FDTD) method [1], or finite-element method (FEM) [2]. For an IE analysis of planar structures in stratified media, a large amount of analytical work can be done by using a spectral-domain approach (SDA) [3], [4] for constructing the required Green's functions. IEs in stratified media are formulated as electric field integral equations (EFIEs) with a dyadic Green's function or as mixed potential integral equations (MPIEs) with scalar and vector potential Green's functions. Reaction integrals [5] for the method of moments (MoM) [6] solution of the IE can be evaluated in the spectral or space domain. The IE/SDA technique has been applied for more complicated geometries, from two-and-one-half-dimensional (2.5-D) structures [7]–[10] to almost fully three-dimensional (3-D) [11]–[14] and complete 3-D structures [15]. Terminology to clearly specify the geometry is given in Section I-A. Either the EFIE [7] or standard available MPIE [11], [13] formulations have been used. In this paper, we propose a hybrid dyadic-mixed-potential field formulation (Section II) specifically adapted to analyze "quasi 3-D" geometries. We also propose a combined spectral–space-domain evaluation of the reaction integrals (Section III). This method extends earlier more limited approaches revised in Section I-B. The dyadic z, z'-dependent parts of all reaction integrals are performed analytically (see Section IV) and evaluated in the spectral domain. After the numerical inverse Fourier transform, the remaining integrals in the transverse coordinates are done with the space-domain MPIE formalism. The evaluation of the reaction integrals and inverse Fourier transform is interleaved depending on the type of coupling. Thus, we combine space- and spectral-domain techniques to deal with the singular behavior of the Green's functions. Section IV shows how the closed-form integrations are done using a factorization (Section IV-B) and general derivative relations (Section IV-B), valid for Green's functions in an arbitrary stratified medium. The numerical results of Section V demonstrate the validity of the proposed techniques for most practical problems that one first thinks of as fully 3-D.

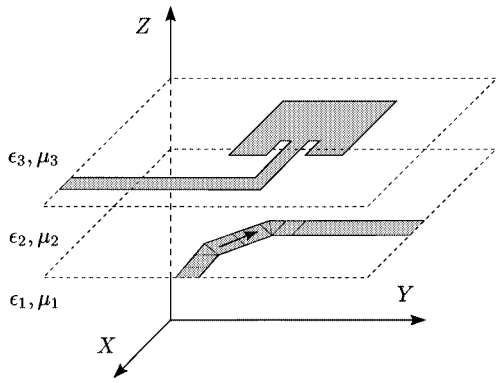

Fig. 1. Familiar 2-D or planar structure.

A. Field Formulations for Two-Dimensional (2-D) to 3-D Problems

Fig. 1 shows the 2-D or planar case. Metal surfaces are strictly horizontal and located at a limited number of discrete z-positions. Theoretically, the field can be cast into MPIE form, as in [16]. Fig. 2 depicts the 2.5-D or "3-D planar" case. A limited capability to model vertical currents is incorporated to analyze probe feeds for patch antennas [17] and via's and air bridges

Manuscript received December 25, 2001; revised May 16, 2002.

The authors are with the Department of Electrical Engineering, Division of Electronics, Systems, Automation, and Technology (ESAT)–Division of Telecommunications and Microwaves (TELEMIC), Katholieke Universiteit Leuven, B-3001 Leuven, Belgium (e-mail: Mark.Vrancken@esat.kuleuven.ac.be).

Digital Object Identifier 10.1109/TMTT.2002.806909

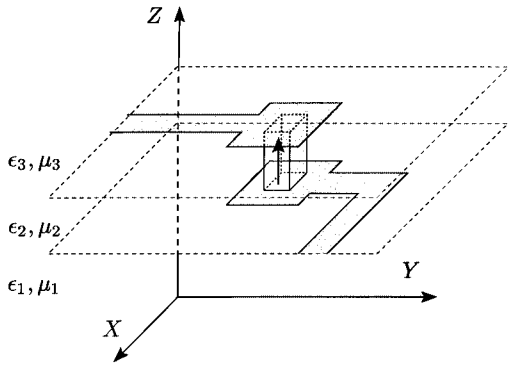

Fig. 2. 2.5-D or 3-D planar structure. Vertical currents are constant and confined to a single dielectric layer.

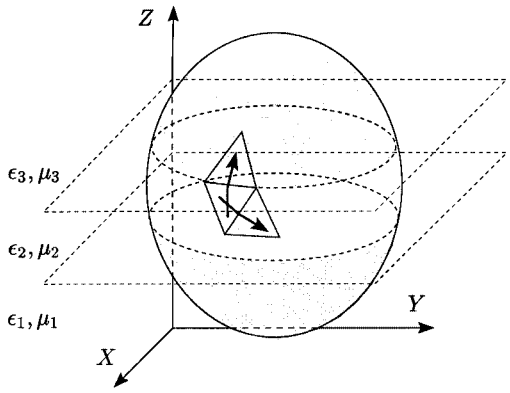

Fig. 3. Fully 3-D structure. An arbitrary curved surface is modeled using currents with arbitrary orientation.

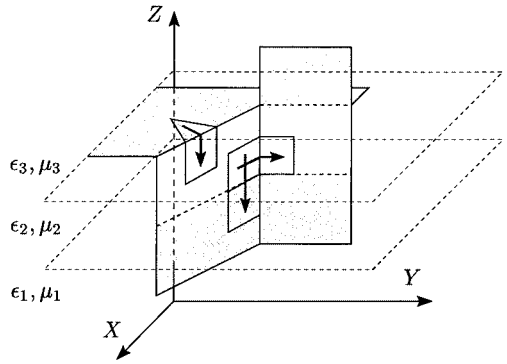

Fig. 4. Quasi-3-D structure composed of horizontal and strictly vertical surfaces. These can cross interfaces between dielectric layers and all current components are modeled.

[10], [11] in planar circuits. Due to the small dimensions, transverse current components on the vertical conductors can be neglected and the remaining z-component can be assumed constant, as in [7], [9], and [10]. The current cannot cross the interface between adjacent dielectric layers. The z-component of the current was introduced into MPIE formulations, as in [17], or added in EFIE form, as in [10]. Several commercial software packages can analyze 2.5-D geometries.[1] [2] [3] [4] Fig. 3 depicts a full 3-D problem [15]. Due to the larger dimensions, the current can no longer be assumed constant and it can have arbitrary orientation at all positions in the layer structure. It can cross the interfaces between adjacent layers. For this case, theoretical difficulties have been experienced in formulating the MPIE: one is confronted with multiple scalar potential kernels [18], [19] or a dyadic vector potential kernel [15]. In the last case, higher order Sommerfeld integrals S_n (see Appendix A) complicate the numerical inverse Fourier transform, and a dependence on the azimuth angle $\phi = \arctan((x-x')/(y-y'))$ strongly complicates the evaluation of the reaction integrals in the space domain [8], [9]. Some commercial software packages offer full 3-D capability.[5] [6] Fig. 4 depicts the quasi-3-D geometry we will concentrate on. Vertical surfaces can be arbitrarily large and can cross dielectric interfaces. The current flowing on the surface is decomposed into vertical and horizontal components. This is not a full 3-D problem since the vertical surface and the current on it cannot have arbitrary inclination unless a staircase approximation is made (not provided in the examples). This geometry was already treated in [12]–[14], but using a total MPIE formulation. For this specific geometry, we propose a hybrid dyadic-mixed-potential formulation in Section II.

B. Space-Domain Approach Versus SDA

For the planar structures of Fig. 1, Green's functions are computed for a limited number of combinations of z, z'-coordinates. This becomes a problem when currents are distributed in a continuous manner over all z, z'-positions. A first engineering approach evaluates the integrals involving varying z, z'-variables numerically in the space domain, interpolating from a set of precalculated Green's functions for a sufficient number of z, z' combinations. This was done for a constant vertical current in a single-layered medium with an EFIE formulation in [7], for quasi-3-D structures in a single layered medium in [11], and for a double-layered medium in [12], both, however, using a total MPIE formulation. For full 3-D problems, this is apparently the method used in IE3D and FEKO confirmed. Care has to be exercised with the continuity of the Green's functions and their derivatives as they cross dielectric interfaces [12], [14]. The interpolation procedure has to be applied for the scalar potential kernel and all components of the dyadic vector potential kernel. This approach becomes computationally very expensive. For quasi-3-D structures, the current flowing on a vertical surface can be decomposed into vertical and horizontal parts such that the z, z'-integrations can be done analytically. This was done for strictly vertical currents in single-layered media in [8] and [9], but the evaluation takes place in the space domain, while [10]

[1] Sonnet ***em*** Suite, *3D Planar High Frequency Electromagnetic Simulation*, Sonnet Software Inc., Syracuse, NY. [Online]. Available: http://www.sonnetusa.com

[2] *Microwave Office 2000*, Applied Wave Research Inc., El Segundo, CA. [Online]. Available: http://www.mwoffice.com

[3] *Momentum Planar Electromagnetic Simulator*, Agilent Technol. EEsof EDA, Agilent Technol., Palo Alto, CA. [Online]. Available: http://www.agilent.com

[4] Ansoft Ensemble, *Planar EM Simulation Software for RF and Wireless Design*, Ansoft Corporation, Pittsburgh, PA. [Online]. Available: http://www.ansoft.com

[5] IE3D *Planar and 3D Electromagnetic Simulation and Optimization Package*, Zeland Software Inc., Fremont, CA. [Online]. Available: http://www.zeland.com

[6] *FEKO, FEldberechnung bei Körpern mit beliebiger Oberfläche, Field Computations Involving Objects of Arbitrary Shape*, EMSS—em Software & Systems Ltd., Stellenbosch, South Africa. [Online]. Available: http://www.emss.co.za

realizes that a spectral-domain evaluation reduces the singular behavior. More recently, [13] modeled vertical and horizontal current components with a spectral-domain evaluation of z, z' integrals for quasi-3-D structures in double-layered media, but again, using a total MPIE formulation. No general expressions for the z, z' integrals for multiple-layered media were obtained [14]. In this study, we evaluate all z, z' integrals in closed form, based on derivative relations and a factorization for Green's function in arbitrarily layered media. The technique is combined with the hybrid field formulation to deal with the Green's function singular behavior. The singularity of the dyadic z, z'-dependent part is reduced by evaluating the closed-form formulas in the spectral domain. In the space-domain MPIE part of the formulation, derivatives are transferred to the basis and test functions. The exact interleaving of closed-form spectral-domain evaluation, numerical inverse Fourier transform, and space-domain MPIE technique depends on the directions of fields and currents and is worked out in Section III.

II. Hybrid Dyadic-Mixed Potential Formulation

The field in an arbitrarily stratified medium is obtained by performing a Fourier transform of the transverse spatial (x, y) coordinates to the (k_x, k_y) wavenumber domain. The spectral-domain counterpart of a spatial function G is written as $\widetilde{G}$. One obtains an equivalent transmission line along the z-direction for the TE and TM parts of the field [4]. Each layer of the medium corresponds to a section k of the equivalent transmission-line system of Appendix B, and is determined by a propagation constant $\gamma_k = \sqrt{k_\rho^2 - \omega^2\mu_k\epsilon_k}$ and characteristic admittance Y_k as follows:

$$Y_k^{\mathrm{TE}} = \frac{\gamma_k}{j\omega\mu_k} \quad Y_k^{\mathrm{TM}} = \frac{j\omega\epsilon_k}{\gamma_k}. \tag{1}$$

All Green' functions can be expressed with the functions

$$\widetilde{F}_{ij}^{S^T}(k_\rho, z, z') \tag{2}$$

where $F = I, V$ is the current or voltage at position z in section i, $S = I, V$ is the unit current or voltage source at position z' in section j, and both $T = \mathrm{TE}, \mathrm{TM}$ systems are also indicated. In the quasi-3-D structures, there are no currents inclined with respect to the X, Y-plane. This allows to avoid the complications of a fully 3-D formulation. Also, in Section IV, the z, z' part of the reaction integrals will be done analytically. It is, therefore, better to express vertical field and current relations in dyadic form. For the horizontal currents, the MPIE formulation retains its usual advantages. Thus, we arrive at

$$\vec{E}_{it} = -j\omega S_0\left\{\frac{\widetilde{V}_{ij}^{I^{\mathrm{TE}}}}{-j\omega}\right\}\vec{J}_{jt} - \nabla_t S_0\left\{j\omega\frac{\widetilde{V}_{ij}^{I^{\mathrm{TE}}} - \widetilde{V}_{ij}^{I^{\mathrm{TM}}}}{k_\rho^2}\right\} \cdot\left(\frac{\nabla_t'\cdot\vec{J}_{jt}}{-j\omega}\right) \tag{3}$$

$$E_{iz} = S_0\left\{\frac{k_\rho^2}{j\omega\epsilon_i j\omega\epsilon_j}\widetilde{I}_{ij}^{V^{\mathrm{TM}}}\right\}J_{jz} \tag{4}$$

while the relations between transverse field and vertical currents and vice versa are expressed in an intermediate fashion

$$\vec{E}_{it} = -\nabla_t S_0\left\{\frac{\widetilde{V}_{ij}^{V^{\mathrm{TM}}}}{j\omega\epsilon_j}\right\}J_{jz} \tag{5}$$

$$E_{iz} = S_0\left\{\frac{1}{\epsilon_i}\widetilde{I}_{ij}^{I^{\mathrm{TM}}}\right\}\left(\frac{\nabla_t'\cdot\vec{J}_{jt}}{-j\omega}\right). \tag{6}$$

Only lowest order Sommerfeld integrals are required and no azimuth angular dependence is present. The only apparent problem is that the function occurring in (4) has a $1/R^3$, and the ones in (5) and (6) have a $1/R^2$ spatial singular behavior, as opposed to the basic $1/R$ singularities of (3). This singular behavior can be reduced, however, by performing part of the reaction integrals already in the spectral domain, prior to the numerical inverse Fourier transform, as described in the next section.

III. Combined SDA-Spatial-Domain Approach for Evaluation of the Reaction Integrals

The IE for the electric field is discretized using a MoM [6] with the by now standard rooftop expansion functions [20]. The elements of the MoM coupling matrix are obtained from the reaction integrals [5]

$$Z_{ij} = -\frac{1}{I_i I_j}\int_S \vec{J}_i \cdot \int_{S'}\vec{E}_i(\vec{J}_j)\,\mathrm{d}S\mathrm{d}S' \tag{7}$$

where the integrals extend over the observation and source surfaces S and S', where $\vec{J}_i$ and $\vec{J}_j$ are nonvanishing. In evaluating these integrals, the currents on the vertical surfaces are expanded with rectangular rooftop functions that are directed strictly vertical or horizontal, as depicted in Fig. 4, such that the z, z'-dependent part can be performed in closed form. Below, we will drop the normalization I_i and I_j and express $\vec{E}_i(\vec{J}_j)$ with a multilayered Green's function.

A. MPIE-Space-Domain Approach

The electromagnetic coupling between transverse $t = x, y$ currents is done in the standard way [16]. Inserting the mixed potential form of (3) into (7) gives

$$Z_{ij}^{tt} = -j\omega\int_S \vec{J}_{it}\cdot\int_{S'} S_0\left\{\frac{\widetilde{V}_{ij}^{I^{\mathrm{TE}}}}{-j\omega}\right\}\vec{J}_{jt}\,\mathrm{d}S'\mathrm{d}S - j\omega\int_S Q_i\int_{S'} S_0\left\{j\omega\frac{\widetilde{V}_{ij}^{I^{\mathrm{TE}}} - \widetilde{V}_{ij}^{I^{\mathrm{TM}}}}{k_\rho^2}\right\}Q_j\,\mathrm{d}S'\mathrm{d}S. \tag{8}$$

The charges Q_i and Q_j are obtained in partial integration procedures where one derivative of the Green's function was transferred to the observation current $\vec{J}_{it}$ and another to the source current $\vec{J}_{jt}$. As a result, both the scalar and vector potential Green's functions have a worst case $e^{-k_\rho/\Delta}k_\rho$ behavior for large k_ρ in the spectral domain, and a corresponding (see Appendix C) $1/\sqrt{\rho^2+\Delta^2}$ singular behavior for small ρ in the spatial domain.

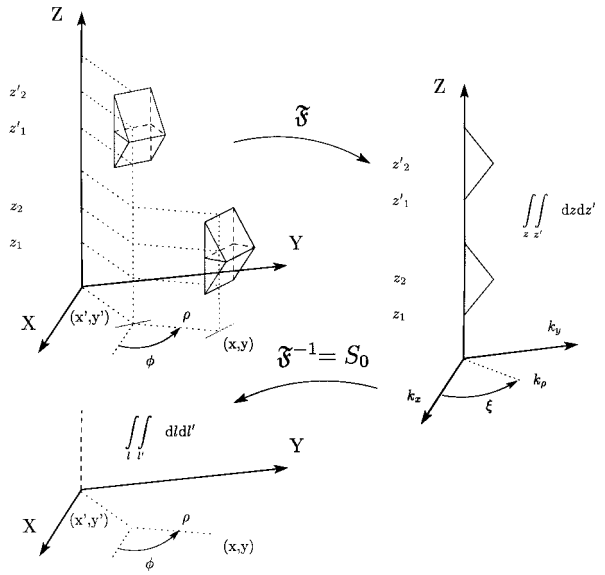

Fig. 5. Combined SDA and spatial-domain approach for the evaluation of the reaction integrals for two vertical currents. Closed-form integration in the spectral domain facilitates the numerical inverse Fourier transform and reduces the singularity in the spatial domain.

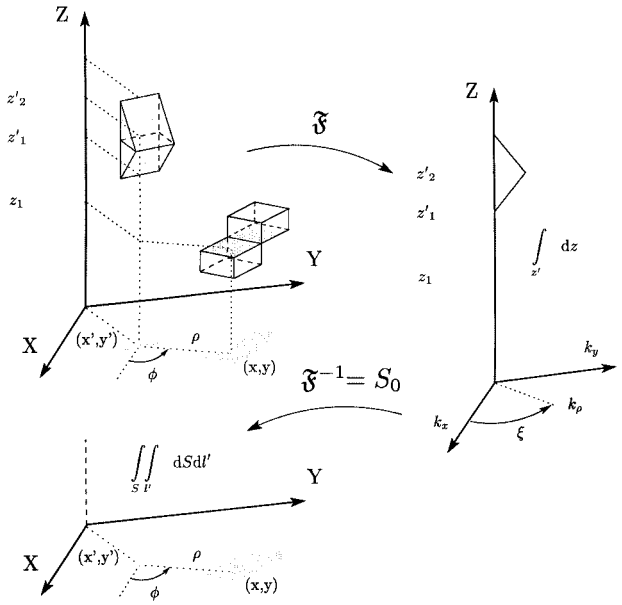

Fig. 6. Combined SDA and spatial-domain approach for the evaluation of the reaction integrals for the coupling of a vertical current to a horizontal current. Notice that only the current is required for the vertical current and only the charge for the horizontal current.

B. Dyadic SDA

To evaluate the reaction integral (7) for vertical currents, we insert (4) into (7) and try to evaluate

$$Z_{ij}^{zz} = \frac{1}{j\omega\epsilon_i} \int_S J_{iz} \int_{S'} S_0 \left\{ k_\rho^2 \frac{\widetilde{I}_{ij}^{V^{\mathrm{TM}}}}{j\omega\epsilon_j} \right\} J_{jz}\, \mathrm{d}S'\mathrm{d}S \qquad (9)$$

but the numerical inverse Fourier transform would be difficult since a $k_\rho e^{-k_\rho \Delta}$ asymptotic behavior in the spectral domain confronts us. A corresponding spatial $1/\sqrt{\rho^2+\Delta^2}^5$ singularity has to be integrated. We, therefore, bring the z, z'-dependent part of the surface integrals "inside" of the inverse Fourier transform

$$Z_{ij}^{zz} = \frac{1}{j\omega\epsilon_i} \iint_{l\,l'} S_0 \left\{ \int_z \widetilde{J}_{iz} \int_{z'} k_\rho^2 \frac{\widetilde{I}_{ij}^{V^{\mathrm{TM}}}}{j\omega\epsilon_j} \widetilde{J}_{jz} \mathrm{d}z'\mathrm{d}z \right\} \mathrm{d}l'\mathrm{d}l \qquad (10)$$

where l, l' are curves in the X,Y-plane. The z, z'-integrations can be performed in closed form with the techniques given in Section IV. The resulting formulas are evaluated in the spectral domain. It will be demonstrated in Section IV-C that these extra integrations improve the asymptotic spectral and spatial singular behavior. For the above case, an improved $e^{-k_\rho\Delta}/k_\rho^2$ and $ln(\Delta + \sqrt{\rho^2+\Delta^2})$ behavior are obtained. The evaluation of the reaction integrals is depicted in Fig. 5. No charges appear in this part of the formulation.

C. Cross-Coupling Terms

For the evaluation of the electromagnetic coupling from a vertical current to a horizontal current, we follow an intermediate way. Inserting (19) into the reaction integral (7)

$$Z_{ij}^{tz} = \int_S \vec{J}_{it} \cdot \nabla_t \int_{S'} S_0 \left\{ -\frac{\widetilde{V}_{ij}^{V^{\mathrm{TM}}}}{j\omega\epsilon_j} \right\} J_{jz}\, \mathrm{d}S'\mathrm{d}S \qquad (11)$$

allows to transfer one derivative to the observation current, and perform one closed-form integration in the spectral domain

$$Z_{ij}^{tz} = \int_S Q_i \int_{l'} S_0 \left\{ \int_{z'} \frac{\widetilde{V}_{ij}^{V^{\mathrm{TM}}}}{\epsilon_j} \widetilde{J}_{jz}\, \mathrm{d}z' \right\} \mathrm{d}l'\mathrm{d}S. \qquad (12)$$

The procedure is visualized in Fig. 6. If the horizontal current flows on a vertical sheet, an additional z integration can be moved "inside" of the inverse Fourier transform and, for this case, the analytical integration will be given completely in (19) of Section IV-C. The reciprocal coupling is dealt with in a similar manner by inserting (6) into (7), and this gives

$$Z_{ij}^{zt} = \int_l \int_{S'} S_0 \left\{ \int_z \widetilde{J}_{iz} \frac{\widetilde{I}_{ij}^{I^{\mathrm{TM}}}}{\epsilon_i}\, \mathrm{d}z \right\} Q_j\, \mathrm{d}S'\mathrm{d}l. \qquad (13)$$

In both cross-coupling formulas, the problematic asymptotic/singular behavior is thus treated by combining the techniques from the two previous cases.

IV. Analytical Integration

The analytical integrations occurring in (10), (12), and (13) are based on a general factorization (Section IV-A) and general derivative relations (Section IV-B) valid for Green's functions in arbitrarily multilayered media.

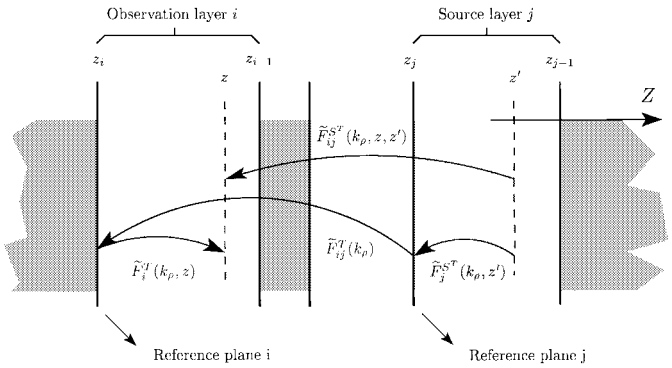

Fig. 7. Factorization of the Green's function into a transfer function and shift functions.

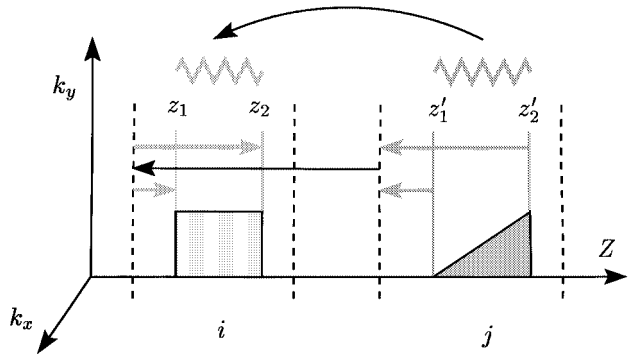

Fig. 8. Analytical integration of the z, z'-dependent part of the reaction integrals.

A. Factorization of the Green's Function

To increase the efficiency of the computation of a set of Green's functions $\widetilde{F}_{ij}^{S^T}(k_\rho, z, z')$, a factorized form has been developed. We choose reference planes on the left-hand side of the layers under consideration at the positions z_i and z_j, as indicated in Fig. 7 (the right-hand side z_{i-1} and z_{j-1} can also be used). An arbitrary Green's function is written as a product of a transfer function $\widetilde{F}_{ij}^T(k_\rho)$ between the chosen reference positions, and shift factors $\widetilde{F}_j^{S^T}(k_\rho, z')$ and $\widetilde{F}_i^T(k_\rho, z)$ for the exact source and observation positions

$$\widetilde{F}_{ij}^{S^T}(k_\rho, z, z') = \widetilde{F}_i^T(k_\rho, z)\,\widetilde{F}_{ij}^T(k_\rho)\,\widetilde{F}_j^{S^T}(k_\rho, z'). \tag{14}$$

The explicit expressions are given in Appendix B. Instead of computing separately all possible combinations z, z', we need only compute the transfer and shift functions once, and then use these values to compute all possible combinations. This is especially profitable for the numerical evaluation as a function of the spectral wavenumber k_ρ, where a large number of evaluations can be required, but it is also used for extraction of the surface wave and branch point singularities, and the asymptotic behavior [21]. In case of the surface wave pole singularity, the residue computation is performed for only one function. The values of the residue coefficients for all other functions follow from reciprocity and the use of the shift and transfer functions evaluated for k_ρ equal to the pole value.

B. Derivative Relations

The Green's functions in a multilayered medium show translational invariance only in the transverse (x, y)-coordinates so we can use $\nabla_t = -\nabla_t'$. More general formulas have to be relied on for the z, z'-coordinates. These follow immediately from the explicit expressions for the factorized Green's functions (14). For derivatives involving the observation z-coordinate, we see from (27) and (28) that

$$\frac{\partial}{\partial z}\widetilde{I}_i^T(z) = -\gamma_i Y_i^T\,\widetilde{V}_i^T(z) \tag{15}$$

$$\frac{\partial}{\partial z}\widetilde{V}_i^T(z) = -\frac{\gamma_i}{Y_i^T}\,\widetilde{I}_i^T(z) \tag{16}$$

which are the usual transmission-line equations (without considering the delta function contributions when $z = z'$). For derivatives to the source z' variable, we obtain from (29)–(32) the reciprocal relations

$$\frac{\partial}{\partial z'}\widetilde{F}_j^{V^T}(z') = -\gamma_j Y_j^T\,\widetilde{F}_j^{I^T}(z') \tag{17}$$

$$\frac{\partial}{\partial z'}\widetilde{F}_j^{I^T}(z') = -\frac{\gamma_j}{Y_j^T}\,\widetilde{F}_j^{V^T}(z') \tag{18}$$

where, instead of the current or voltage itself, the source type changes. This set of relations is essential for easy manipulation and computation of the closed-form integrals of Section IV-C.

C. Analytical Integration

The derivative relations (15)– (18) can now be used in a partial integration procedure involving Green's functions and standard rooftop functions. Together with the factorized form of (14), this gives clear analytical formulas. For example, in Fig. 8, we consider the electromagnetic coupling from a vertical current to a horizontal current also flowing on a vertical surface. Both currents are expanded using rooftop functions, but for the horizontal current, the z dependence is a constant function. The result of the computation is

$$\begin{aligned}\int_{z_1}^{z_2}\int_{z_1'}^{z_2'} 1\frac{z'-z_1'}{z_2'-z_1'}\left\{-\frac{\widetilde{V}_{ij}^{\mathrm{TM}}}{j\omega\epsilon_j}\right\}\mathrm{d}z'\mathrm{d}z \\ = -\frac{1}{\gamma_j^2}\delta\left[z_2' \le z \le z_1'\right] + \frac{1}{j\omega\epsilon_i}\left[\widetilde{I}_i^{\mathrm{TM}}(z_2) - \widetilde{I}_i^{\mathrm{TM}}(z_1)\right] \\ \cdot\,\widetilde{I}_{ij}^{\mathrm{TM}}\left[\frac{\widetilde{I}_j^{I^{\mathrm{TM}}}(z_2')}{\gamma_j^2} + \frac{1}{\gamma_j^2}\frac{\widetilde{I}_j^{V^{\mathrm{TM}}}(z_2') - \widetilde{I}_j^{V^{\mathrm{TM}}}(z_1')}{j\omega\epsilon_j\,|\,z_2' - z_1'\,|}\right]\end{aligned} \tag{19}$$

where the δ-functions appears if the basis functions in Fig. 8 overlap. It arises by taking into account the discontinuous behavior of the voltages and currents on the transmission-line system described in Appendix B at the source position or by explicitly including δ-functions in (15)–(18). Notice that the z integration only affects the observation shift function, while z' integration only affects the source shift function. These parts can be recognized in (19) and Fig. 8. The analytical integrations can change the observation $F = I, V$ and/or source type $S = I, V$ of the expressions and/or can introduce factors $1/\gamma_i^2$ and $1/\gamma_j^2$. These factors do no introduce any extra singularities in the spectral domain (as can be verified by expanding the

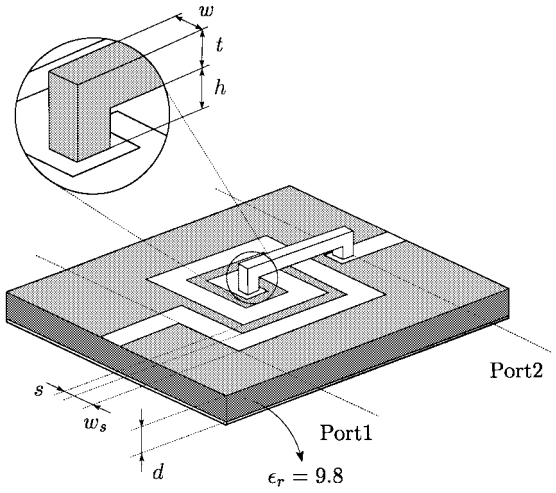

Fig. 9. Microstrip rectangular spiral inductor with an air bridge that will be modeled with a zero and finite thickness.

expressions in series for $k_\rho = k_i, k_j$), but do improve the spectral decay since, for large spectral values, they behave as

$$\lim_{k_\rho \to \infty} \gamma_i = \lim_{k_\rho \to \infty} \sqrt{k_\rho^2 - k_i^2} = k_\rho. \tag{20}$$

Thus, the closed-form integrations always improve the asymptotic spectral behavior.

V. Examples

A. Microstrip Inductor With Air Bridge

In the first example, we investigate the influence of the finite thickness of the upper piece of the air bridge of a microstrip rectangular spiral inductor. The structure is depicted in Fig. 9. The feeding microstrip lines are characterized by $d = 635\,\mu$m, $w_s = 625\,\mu$m, and $\epsilon_r = 9.8$. The spacing between the turns of the spiral is $s = 312.5\,\mu$m. The thicknesses of the vertical studs and the height of the air bridge are $w = h = 312.5\,\mu$m, while the thickness of the upper piece of the air bridge is compared for $t = 0\,\mu$m or $t = 312.5\,\mu$m. The example was originally introduced in [22]. Measurements were performed on a structure where the air bridge was actually a wire with circular cross section of diameter 317.5 μm. An IE analysis was done in [7], where the vertical pieces of the air bridge are modeled with constant vertical currents, and the horizontal piece is an infinitely thin flat strip. An improved analysis is done in [11], where allcomponents of the current were modeled using the common MPIE formulation and the finite thickness is taken into account. We have taken the simulated results of [11] as reference curves in the following graphs. Fig. 10 shows amplitude and phase of S_{22} as we computed them in 145 frequency points from 2.0 to 20.0 GHz for $t = 0\,\mu$m. The slight shift that occurs when the upper piece is modeled as a box is given in the same format in Fig. 11.

B. Cavity-Backed Antenna With Superstrate

Fig. 12 depicts a cavity-backed patch antenna with a dielectric superstrate. The dimensions of the patch are $W_p = 1.5\,$cm and $L_p = 1.5\,$cm. The size of the cavity is $W_a = 1.875\,$cm, $L_a = 1.875\,$cm, and a depth $H_a = 0.9375\,$cm. The dielectric overlay has thickness $t = 0.7874\,$mm and $\epsilon_r = 2.22$ or $\epsilon_r = 1.00$. The inner conductor of the coaxial feed terminates on the middle of the patch. In [23], the analysis was performed with a magnetic current in the region between the patch and infinite ground plane. A dyadic Green's function for the magnetic current was used in the upper dielectric region and inside the rectangular cavity. The feed was a delta gap voltage generator. To show the validity of our approach, we perform the dual analysis by computing all electric currents. The bottom of the cavity is our infinite ground plane, while the current on the patch, cavity sidewalls, and upper ground plane is expanded with rooftop functions. The upper ground plane is necessarily finite in our approach ($W_g = L_g = 48.75\,$mm). Our excitation is a current source connecting the patch to the surrounding ground plane. Of course, the analysis of [23] is much more efficient for this particular case, but is limited to strictly rectangular closed cavities. Our computation can handle arbitrarily shaped cavities with possible openings in the cavity walls. In Fig. 13, we repeat some results of [23] for reference purposes. One clearly sees the effect of the superstrate on the input impedance. We reproduce these computations and compare them with the measured results of [23] in Fig. 14. A slight shift in frequency can be observed. This might be due to different feed models since a further increase of the size of the ground plane or refinement of the mesh gives no further significant improvement of the results.

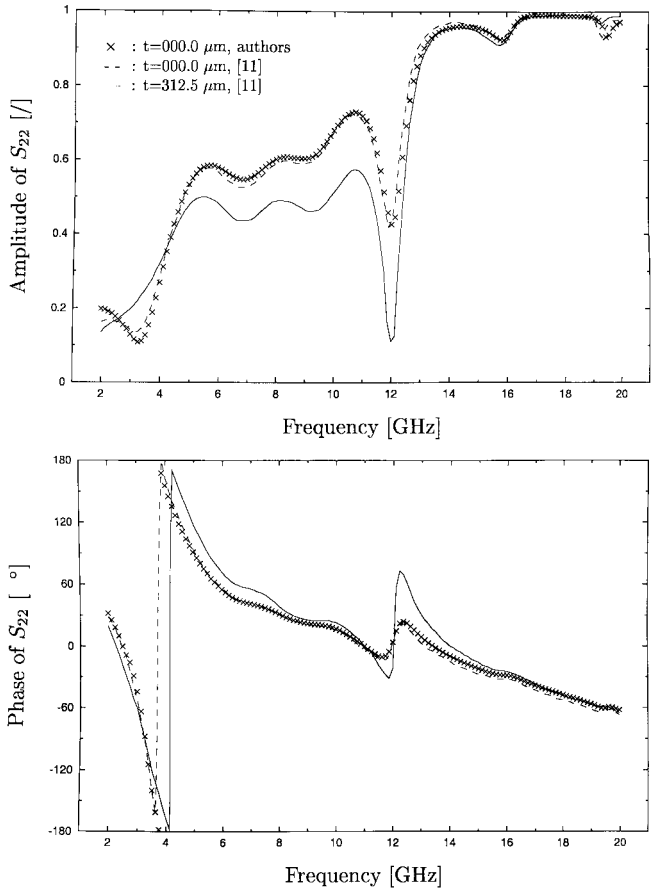

Fig. 10. Amplitude and phase of S_{22} in 145 points in the frequency range from 2.0 to 20.0 GHz. Thickness of the upper piece of the air bridge is $t = 000.0\,\mu$m for our computed results.

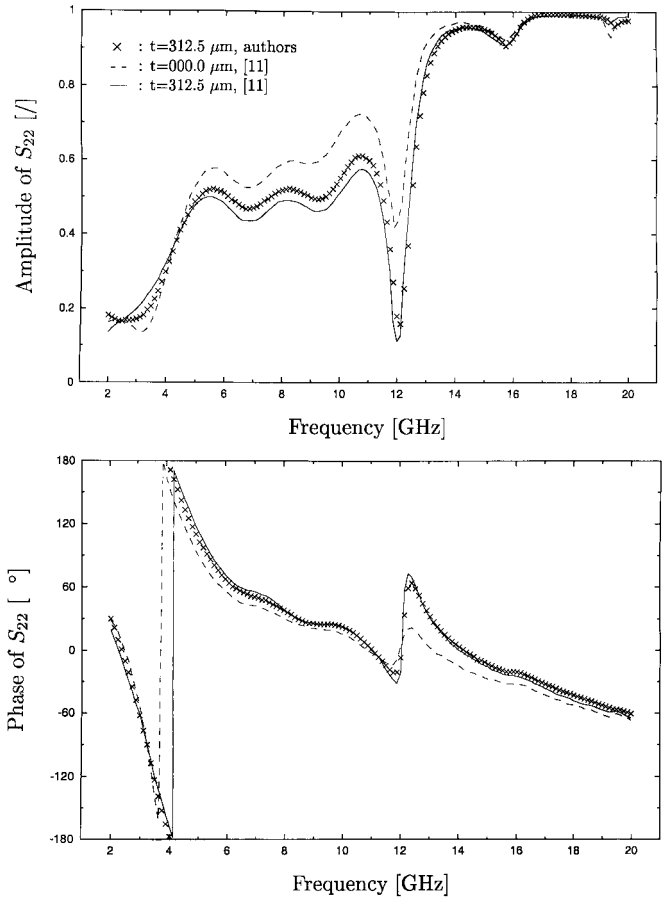

Fig. 11. Amplitude and phase of S_{22} in 145 points in the frequency range from 2.0 to 20.0 GHz. Thickness of the upper piece of the air bridge is $t = 312.5\ \mu$m for our computed results.

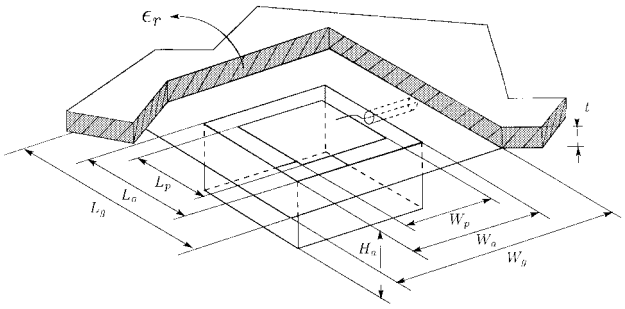

Fig. 12. Coaxially fed cavity-backed patch antenna with a dielectric overlay.

C. Packaged Monolithic Microwave Integrated Circuits (MMICs)

The behavior of MMICs packaged in a metallic box, as depicted in Fig. 15, can deviate from the original unpackaged behavior due to box resonances and proximity effects of the sidewalls. The sharp resonance effects can be combated by introducing absorbing materials such as the lossy layer attached to the cover of the box in Fig. 15. Nevertheless, there usually remain frequency shifts and other perturbations of the circuit response. For the circuit in Fig. 15, the shunt stub with $w = 1.4\,$mm and $l = 1.9\,$mm originally has a stopband around 11 GHz, and this behavior is not altered much when the circuit is positioned at $x_c = 7.5\,$mm and $y_c = 17\,$mm. The example

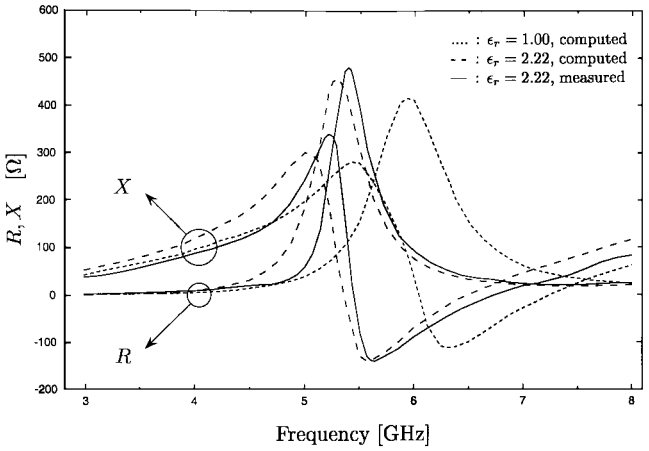

Fig. 13. Input impedance R + jX of the antenna of Fig. 12 with and without dielectric overlay, as computed and measured by [23] (3.0–8.0 GHz).

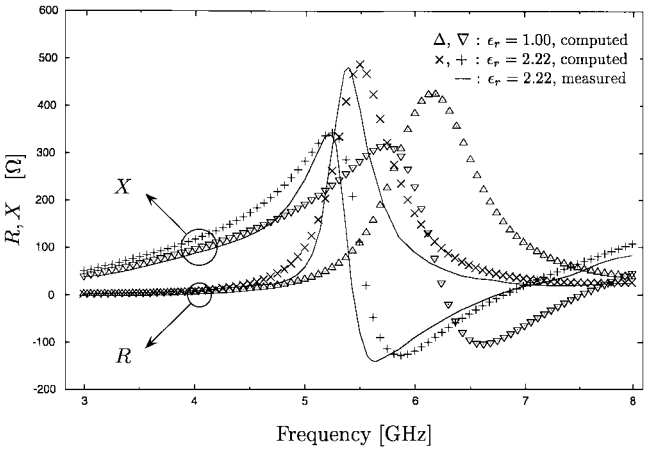

Fig. 14. Input impedance $R + jX$ of the antenna of Fig. 12 with an without dielectric overlay computed in 81 frequency points for 3.0–8.0 GHz and compared with the measurements of [23].

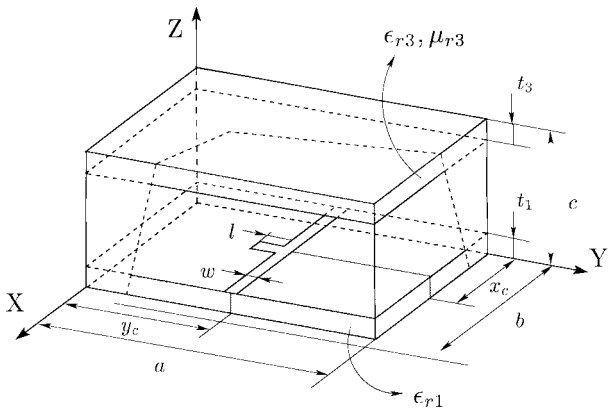

Fig. 15. Studying the effect of the metallic package and absorbing materials on the circuit behavior of the MMIC.

is taken from [24]. The box has dimensions $a = 15\,$mm, $b = 24\,$mm, and $c = 12.7\,$mm and covers the circuit on a substrate of $t_1 = 1.27\,$mm and $\epsilon_{r1} = 10.5(1 - j0.0023)$. The absorbing layer has $t_3 = 1.27\,$mm and $\epsilon_{r3} = 21(1 - j0.02)$, $\mu_{r3} = 1.1(1 - j1.4)$. Fig. 16 compares the results of [24] with our own computations for the amplitude of S_{21} from 9.0 to

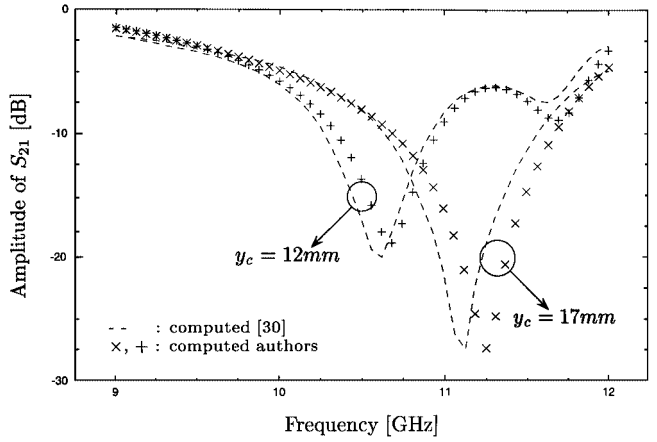

Fig. 16. Amplitude of S_{21} for the boxed circuit of Fig. 15 as computed in 49 points in the frequency range of 9.0–12.0 GHz. The response is influenced by the location y_c in the box.

12.0 GHz in 49 points. When the circuit is moved to the middle of the box at $y_c = 12\,\text{mm}$, the excitation of a box resonance around 10.8 GHz significantly alters the overall behavior, as can be seen in Fig. 16. The results of [24] were computed with a "boxed" Green's function, where the effect of the sidewalls is incorporated in the formulation. In our analysis, the current on the vertical walls of the box was completely expanded using rooftop functions, while the top cover is a part of the layer structure.

D. Overview Computational Effort

Table I gives an overview of problem size, required computer memory, and execution time. The data refer to computations performed on an HP J6000 UNIX workstation with a 552-MHz processor and 1-GB RAM memory. Dense meshing was typically imposed by geometrical features and then extended across the entire structure to maintain a similar cell size everywhere. The problem size is further subdivided into the number of rooftops on horizontal and vertical surfaces and "cornered" rooftops on connections. This relates directly to parts of the computation time per frequency point. Matrix fill time is separated into the spectral part plus numerical inverse Fourier transform and the spatial part. The resulting linear system was solved with an LU decomposition. Additional attention should be spent on increasing efficiency: using discrete complex images (DCIMs) and fast Hankel transform (FHT) techniques for the numerical inverse Fourier transform and exploiting symmetry to reduce the number of reaction integrals that has to be evaluated.

VI. Conclusions

The electromagnetic field in an arbitrarily stratified medium has been given in a hybrid dyadic–mixed potential form. The formulation is particularly well suited to deal with quasi-3-D structures in which currents flow on horizontal and strictly vertical conducting surfaces. The formulation avoids typical problems that hamper total MPIE formulations such as the occurrence of higher order Sommerfeld integrals and an azimuth angular dependence of the components of the dyadic vector potential. The reaction integrals were evaluated in a way that blends the traditional spatial-domain approach and SDA. All integrals involving z, z' variables are done in closed form in the spectral domain prior to the numerical inverse Fourier transform. This is possible due to general derivative relations and a general factorization valid for arbitrary Green's functions. Numerical results illustrate the capabilities of the developed software and the fact that the proposed method can deal with almost all problems in circuits and antennas that one first considers as fully 3-D.

Appendix A

The inverse Fourier transforms of $\widetilde{G}$ and combinations like $k_x\widetilde{G}$, $k_x^2\widetilde{G}$, and $k_xk_y\widetilde{G}$ can be evaluated with Sommerfeld integrals (see [15] for full details)

$$S_n\left\{\widetilde{G}(k_\rho)\right\} = \frac{1}{2\pi}\int_0^{+\infty} \widetilde{G}(k_\rho)\,J_n(k_\rho\rho)\,k_\rho^{n+1}\mathrm{d}k_\rho \qquad (21)$$

where $\rho = \sqrt{\Delta x^2 + \Delta y^2}$, $k_\rho = \sqrt{k_x^2 + k_y^2}$ and J_n the Bessel function of the first kind and order n.

Appendix B

Fig. 17 depicts the equivalent transmission-line system for a planar stratified medium. The unit voltage and current sources $V_S = 1V$, $I_S = 1A$ are located in layer j at position z'. The observation point is in layer i at position z. The characteristic admittance Y_k of section k is defined in (1). We define two sets of impedances and reflection coefficients valid for z-positions $z_k \le z \le z_{k-1}$. The first set $\Gamma_k^>(z), Y_k^>(z)$ is computed starting from the right-hand side. $\Gamma_1(z_0)$ at the outermost right interface 0 is known because of the unbounded medium or metallic ground plane. Using

$$Y_k^>(z) = Y_k\frac{1-\Gamma^>(z)}{1+\Gamma^>(z)} \qquad (22)$$

and continuity of the admittance over the interfaces $z = z_k$, we can compute the value at all positions z in the layer structure. The second set $\Gamma_k^<(z)$ and $Y_k^<(z)$ is obtained in a similar manner, but starts from the left-hand side from the known value of $\Gamma_N(z_{N-1})$ at the outermost left interface, and uses continuity at the interfaces and

$$Y_k^<(z) = Y_k\frac{1-\Gamma^<(z)}{1+\Gamma^<(z)}. \qquad (23)$$

The Green's functions can now be expressed in factorized form, as in (14), where the explicit expressions for F, $S = I$, and V are given only for the case when the reference interfaces are located at z_i and z_j and the observation point z is located left of the source position z'. For this particular case, the transfer functions $\widetilde{F}_{ij}$ are

$$\widetilde{V}_{ij} = \prod_{k=j}^{I-1}\frac{1+\Gamma_k^<(z_k)}{e^{-\gamma_k d_k} + \Gamma_k^<(z_k)e^{+\gamma_k d_k}} \qquad (24)$$

$$\widetilde{I}_{ij} = \prod_{k=j}^{I-1}\frac{1-\Gamma_k^<(z_k)}{e^{-\gamma_k d_k} - \Gamma_k^<(z_k)e^{+\gamma_k d_k}}. \qquad (25)$$

TABLE I
OVERVIEW OF COMPUTATIONAL EFFORT FOR EXAMPLES OF SECTION V

	Inductor (t=312.5 μm)	Cavity backed ($\epsilon_r = 2.22$)	Packaged MMIC
# unknowns + right hand sides	1613 + 20	1808 + 1	2394 + 14
Horizontal	1325 + 20	1275 + 1	132 + 14
Vertical	192	451	2106
Connections	96	82	156
execution time per frequency point	4 min 40 sec	4 min 15 sec	15 min 35 sec
Spectral + S_0	1 min 40 sec	2 min 45 sec	13 min 10 sec
Spatial	2 min 50 sec	1 min 15 sec	1 min 50 sec
LU decomposition	10 sec	15 sec	35 sec
maximum RAM	80 MB	90 MB	340 MB

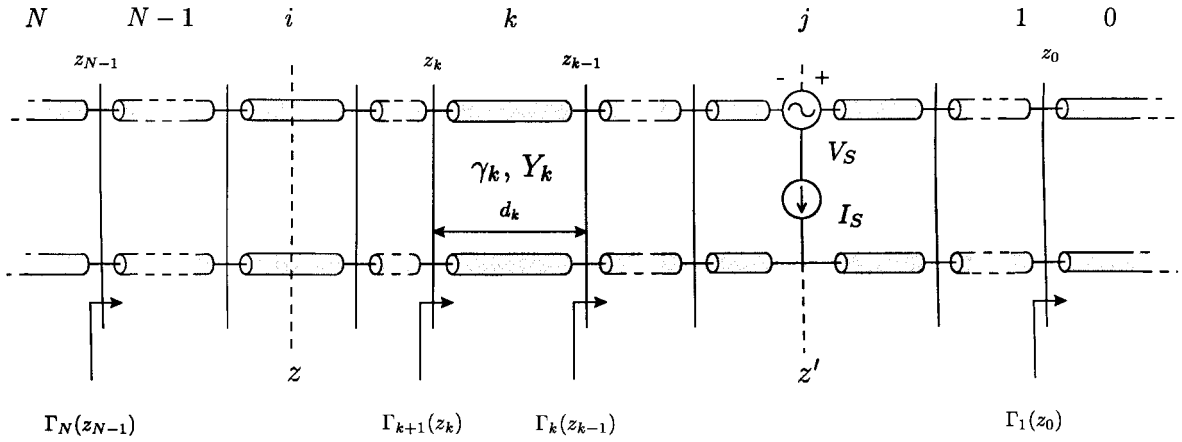

Fig. 17. Equivalent transmission-line system for a stratified medium. The unit sources are located at z' in layer j, and the field is measured at position z in layer i. Each section is determined by the propagation constant γ_k and its characteristic admittance Y_k. This system has to be considered for both the TE and TM fields.

where $d_k = z_k - z_{k-1}$ is the length of section k. Using a simplified notation

$$Y_k^{>} = Y_k^{>}(z_k) \quad Y_k^{<} = Y_k^{<}(z_k) \tag{26}$$

the observation shift functions $\widetilde{F}_i(z)$ are

$$\widetilde{V}_i(z) = \left(Y_i + Y_i^{<}\right)e^{-\gamma_i(z-z_i)} + \left(Y_i - Y_i^{<}\right)e^{+\gamma_i(z-z_i)} \tag{27}$$

$$\widetilde{I}_i(z) = \left(Y_i + Y_i^{<}\right)e^{-\gamma_i(z-z_i)} - \left(Y_i - Y_i^{<}\right)e^{+\gamma_i(z-z_i)} \tag{28}$$

while the source shift functions $\widetilde{F}_j^S(z')$ are given in the following:

$$\widetilde{V}_j^I(z') = \frac{1}{2Y_j}\left(\left(Y_j+Y_j^{<}\right)e^{+\gamma_j(z'-z_j)}+\left(Y_j-Y_j^{<}\right)e^{+\gamma_j(z'-z_j)}\right) \times \frac{1}{Y_j^{<}-Y_j^{>}} \tag{29}$$

$$\widetilde{I}_j^V(z') = \frac{1}{2}\left(\left(Y_j+Y_j^{<}\right)e^{+\gamma_j(z'-z_j)}-\left(Y_j-Y_j^{<}\right)e^{+\gamma_j(z'-z_j)}\right) \times \frac{Y_j^{>}}{Y_j^{<}-Y_j^{>}} \tag{30}$$

$$\widetilde{V}_j^V(z') = \frac{1}{2}\left(\left(Y_j+Y_j^{<}\right)e^{+\gamma_j(z'-z_j)}-\left(Y_j-Y_j^{<}\right)e^{+\gamma_j(z'-z_j)}\right) \times \frac{1}{Y_j^{<}-Y_j^{>}} \tag{31}$$

$$\widetilde{I}_j^I(z') = \frac{1}{2Y_j}\left(\left(Y_j+Y_j^{<}\right)e^{+\gamma_j(z'-z_j)}+\left(Y_j-Y_j^{<}\right)e^{+\gamma_j(z'-z_j)}\right) \times \frac{Y_j^{>}}{Y_j^{<}-Y_j^{>}} \tag{32}$$

Similar expressions are valid when the reference interfaces are located at z_{I-1}, z_{j-1} and when the observation is at the right-hand side of the source.

APPENDIX C

The following Fourier transform pairs give the correspondence between the asymptotic behavior for large k_ρ in the spectral domain and the singular behavior for small transverse distances ρ in the spatial domain. The distance $|z - z'|$ is written as Δ as follows:

$$S_0\left\{k_\rho e^{-k_\rho \Delta}\right\} = \frac{3}{\sqrt{\rho^2+\Delta^2}^5} \tag{33}$$

$$S_0\left\{e^{-k_\rho \Delta}\right\} = \frac{1}{\sqrt{\rho^2+\Delta^2}^3} \tag{34}$$

$$S_0\left\{\frac{e^{-k_\rho \Delta}}{k_\rho}\right\} = \frac{1}{\sqrt{\rho^2+\Delta^2}} \tag{35}$$

$$S_0\left\{\frac{e^{-k_\rho \Delta}}{k_\rho^2}\right\} = \ln\left(\Delta+\sqrt{\rho^2+\Delta^2}\right) \tag{36}$$

REFERENCES

[1] A. Taflove, *Computational Electrodynamics: The Finite Difference Time Domain Method*. Norwood, MA: Artech House, 1997, p. 599.

[2] J. L. Volakis, A. Chatterjee, and L. C. Kempel, *Finite Elements for Electromagnetics*, ser. IEEE/OUP Electromagn. Wave Theory. Piscataway, NJ: IEEE Press, 1997.

[3] R. H. Jansen, "The spectral-domain approach for microwave integrated circuits," *IEEE Trans. Microwave Theory Tech.*, vol. MTT-33, pp. 1043–1056, Oct. 1985.

[4] T. Itoh, "Spectral domain immittance approach for dispersion characteristics of generalized printed transmission lines," *IEEE Trans. Microwave Theory Tech.*, vol. MTT-28, pp. 733–736, July 1980.

[5] V. H. Rumsey, "Reaction concept in electromagnetic theory," *Phys. Rev.*, vol. 94, pp. 1483–1491, Jun. 1954.

[6] R. F. Harrington, *Field Computation by Moment Methods*, ser. Elect. Sci.. New York: Mcmillan, 1968, p. 229.

[7] T. Becks and I. Wolff, "Analysis of 3-D metallization structures by a full-wave spectral domain technique," *IEEE Trans. Antennas Propagat*, vol. 40, pp. 2219–2227, Dec. 1992.

[8] T. Vaupel and V. Hansen, "Electrodynamic analysis of combined microstrip and coplanar/slotline structures with 3-D components based on a surface/volume integral-equation approach," *IEEE Trans. Microwave Theory Tech.*, vol. 47, pp. 1788–1800, Sept. 1999.

[9] N. Kinayman and M. I. Aksun, "Efficient use of closed form Green's functions for the analysis of planar geometries with vertical connections," *IEEE Trans. Microwave Theory Tech.*, vol. 45, pp. 593–603, May 1997.

[10] M.-J. Tsai, C. Chen, N. G. Alexopoulos, and T.-S. Horng, "Multiple arbitrary shape via-hole and air-bridge transitions in multilayered structures," *IEEE Trans. Microwave Theory Tech.*, vol. 44, pp. 2504–2511, Dec. 1996.

[11] R. Bunger and F. Arndt, "Efficient MPIE approach for the analysis of three-dimensional microstrip structures in layered media," *IEEE Trans. Antennas Propagat.*, vol. 45, pp. 1141–1153, Aug. 1997.

[12] P. Gay-Balmaz and J. R. Mosig, "3D planar radiating structures in stratified media," *Microwave Millimeter Wave Computer-Aided Eng.*, vol. 7, pp. 330–343, 1997.

[13] T. M. Gregorczyk, A. K. Skrivervik, and J. R. Mosig, "A full-wave treatment of microstrip antennas containing vertical metallizations," in *Proc. IEEE AP-S Millennium Conf.*, Switzerland, Apr. 9–14, 2000, pp. 280–284.

[14] T. M. Gregorczyk, "Integrated 3D antennas for millimeter-wave applications: Theoretical study and technological realization," Ph.D. dissertation, Dept. Elect., École Polytech. Fédérale de Lausanne, Lausanne, Switzerland, 2000.

[15] K. A. Michalski and D. Zheng, "Electromagnetic scattering and radiation by surfaces of arbitrary shape in layered media, part I: Theory," *IEEE Trans. Antennas Propagat.*, vol. 38, pp. 334–335, Mar. 1990.

[16] J. R. Mosig, "Arbitrarily shaped microstrip structures and their analysis with a mixed potential integral equation," *IEEE Trans. Microwave Theory Tech.*, vol. 36, pp. 314–323, Feb. 1988.

[17] G. A. E. Vandenbosch and A. R. Van de Capelle, "Mixed-potential integral expression formulation of the electric field in a stratified dielectric medium-application to the case of a probe current source," *IEEE Trans. Antennas Propagat.*, vol. 40, pp. 806–817, July 1992.

[18] A. Erteza and B. K. Park, "Nonuniqueness of resolution of Hertz vector in presence of a boundary, and the horizontal dipole problem," *IEEE Trans. Antennas Propagat.*, vol. AP-17, pp. 376–378, May 1969.

[19] K. A. Michalski, "On the scalar potential of a point charge associated with a time-dependent harmonic dipole in a layered medium," *IEEE Trans. Antennas Propagat.*, vol. 35, pp. 1299–1301, Nov. 1997.

[20] S. M. Rao, D. R. Wilton, and A. W. Glisson, "Electromagnetic scattering by surfaces of arbitrary shape," *IEEE Trans. Antennas Propagat.*, vol. AP-30, pp. 409–418, May 1982.

[21] F. J. Demuynck, G. A. E. Vandenbosch, and A. R. Van de Capelle, "The expansion wave concept—Part I: Efficient calculation of spatial Green's functions in a stratified dielectric medium," *IEEE Trans. Antennas Propagat.*, vol. 46, pp. 397–406, Mar. 1998.

[22] M. Rittweger and I. Wolff, "Analysis of complex passive (M)MIC-components using the finite difference time domain method," in *IEEE MTT-S Int. Microwave Symp. Dig.*, Dallas, TX, 1990, pp. 1147–1150.

[23] J.-Y. Lee, T.-S. Horng, and N. G. Alexopoulos, "Analysis of cavity-backed aperture antennas with a dielectric overlay," *IEEE Trans. Antennas Propagat.*, vol. 42, pp. 1556–1562, Nov. 1994.

[24] J. J. Burke and R. W. Jackson, "Reduction of parasitic coupling in packaged MMIC's," in *IEEE MTT-S Int. Microwave Symp. Dig.*, May 1990, pp. 255–259.

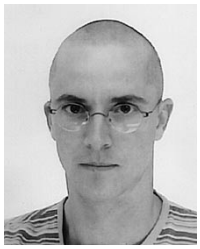

Mark Vrancken (M'96) was born in Herk-de-Stad, Belgium, on January 24, 1973. He received the M.Sc. degree in electrical engineering from the Katholieke Universiteit Leuven, Leuven, Belgium, in 1996, and is currently working toward the Ph.D. degree in numerical modeling of high-frequency electromagnetics in antennas, circuits, and interconnections at the Katholieke Universiteit Leuven.

He is currently a Research Assistant with the Department of Electrical Engineering: Electronics, Systems, Automation, and Technology (ESAT)–Division of Telecommunications and Microwaves (TELEMIC), Katholieke Universiteit Leuven.

Mr. Vrancken was the recipient of a Flemish Institute for the Promotion of Scientific and Technological Research in the Industry (IWT) scholarship from January 1997 to December 2000.

Guy A. E. Vandenbosch (M'85) was born in Sint-Niklaas, Belgium, on May 4, 1962. He received the M.S. and Ph.D. degrees in electrical engineering from the Katholieke Universiteit Leuven, Leuven, Belgium, in 1985 and 1991, respectively.

From 1985 to 1991, he was a Research and Teaching Assistant with the Telecommunications and Microwaves Section, Katholieke Universiteit Leuven, where he was involved with the modeling of microstrip antennas with the IE technique. From 1991 to 1993, he was a Post-Doctoral Researcher with the Katholieke Universiteit Leuven. He is currently a Professor at the same university. His research interests are in the area of electromagnetic theory, computational electromagnetics, planar antennas and circuits, electromagnetic radiation, electromagnetic compatibility, and bioelectromagnetics. His research has been published in international journals and presented at international conferences.

Dr. Vandenbosch is a member of the Management Committee of the European project COST 284 on "Innovative Antennas for Emerging Terrestrial and Space-based Applications." Within this project, he has led the working group on "Models for antennas and RF circuit components." Since 2001, he has been the President of SITEL, the Belgian Society of Engineers in Telecommunications and Electronics. He also currently holds the position of vice-chairman of the IEEE Benelux Chapter on Antennas and Propagation.